Supporting Information

An easy-to-implement combinatorial approach involving an activity-based assay for the discovery of a peptidyl copper complex mimicking superoxide dismutase

Amandine Vincent,[a] Jennifer Rodon Fores,[a] Elodie Tauziet,[a] Elodie Quévrain,[a] Ágnes Dancs,[b] Amandine Conte-Daban,[c] Anne-Sophie Bernard,[a] Philippe Pelupessy,[a] Koudedja Coulibaly,[a] Philippe Seksik,[d] Christelle Hureau,[c] Katalin Selmeczi,[b] Clotilde Policar*[a] and Nicolas Delsuc*[a]

Contents

1. Supplementary scheme

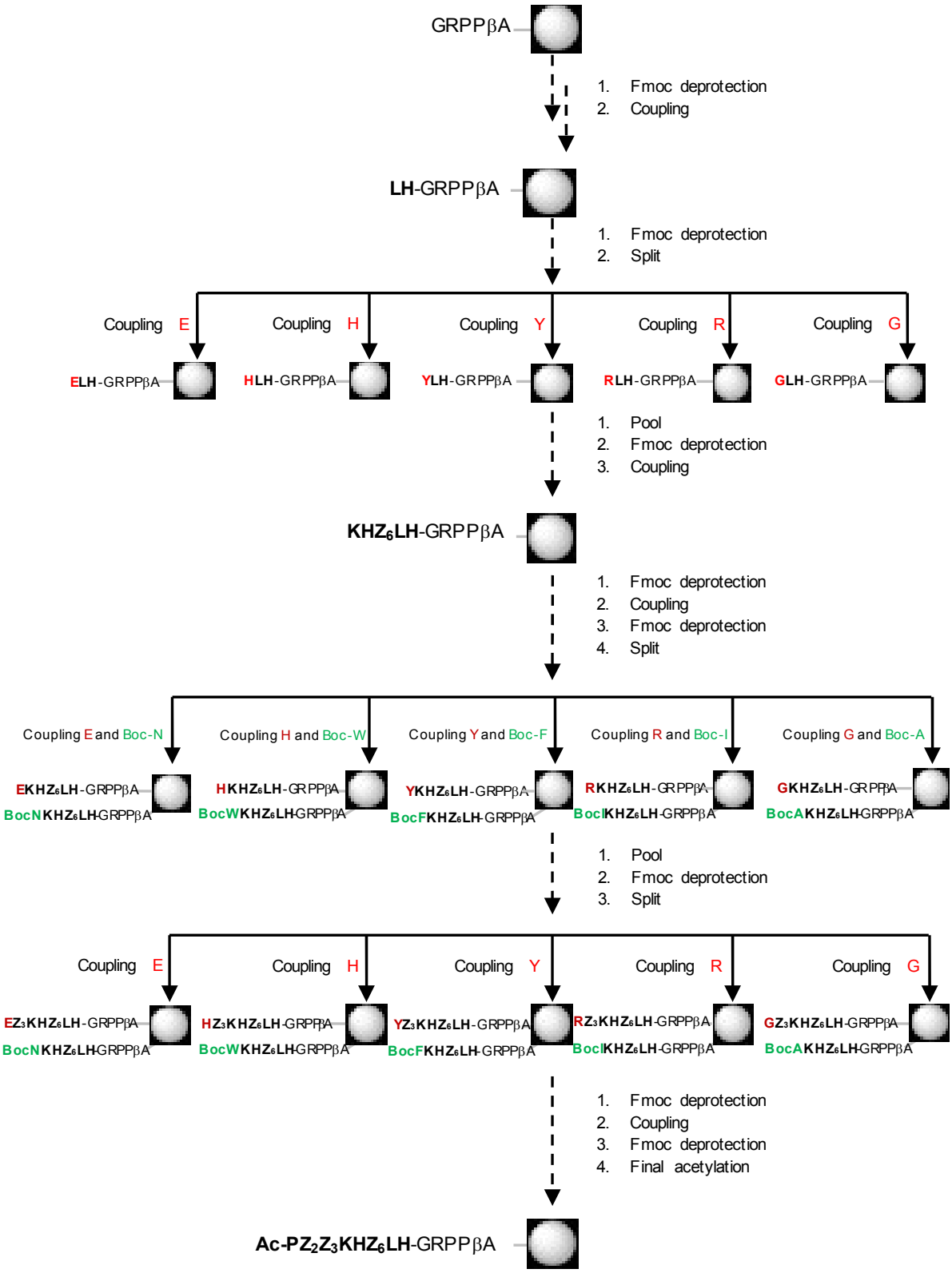

Scheme S1. Library Synthesis using a split and mix strategy.

2. Supplementary tables

Ligand L L/Cu ratio	IC_{50} (µM)	$k_{app}{}_{MCF}{}^{g}$ ($M^{-1}s^{-1}$)	E (V) /NHE	Coordination sphere	Reference
OCP1					
1/1	0.124[a]	$2.3.10^7$	E_{pa} = 0.55 E_{pc} = -0.05	$3N_{im}$,$1N^-$ and $2N_{im}$, $2N^-$	this article
5/1	0.060 [a]	$4.8.10^7$			
Ac-HVH-NH_2					
1/1	0.160[b] 0.160[a]	$1.5.10^7$		$2N_{im,}$ $2N^-$	1 this article
cHH-OH					
2/1	0.500[c]	$4.8.10^7$		$4N_{im}$	2,3
Ac-HHGH-OH					
1/1	0.130[d] 0.150[e]	$2.2.10^7$ $2.0.10^7$		$3N_{im}$,OH^- or $2N_{im}$,N^-,H_2O	4,5
10/1	0.250[e]	$1.2.10^7$			
HADHDHKK-NH_2					
1/1	0.110[c]	$2.7.10^7$		$3N_{im}$, NH_{2term}	6
Ac-HAAHGH-NH_2					
1/1	0.048[f]	$6.2.10^7$	$E_{1/2}$ = 0.33	$2N_{im}$, N^-	4
CuZnSOD	0.0016 [a]	$1.8.10^9$	$E_{1/2}$ = 0.12-0.3	4 N_{im}	this article, 5,7,8
$CuSO_4$	0.603 [a]	$4.8.10^6$			this article

Table S1. Thermodynamic and kinetics constants of representative Cu^{2+} complexes involving a peptidyl ligand.

	Occurrence
AcP**DH**K**HH**L**H**	4
AcPG**E**K**HE**L**H**	2
AcP**DE**K**HE**L**H**	2
AcP**HE**K**HE**L**H**	2
AcP**DE**K**H**GL**H**	2
AcP**DE**K**HE**L**H**	2
AcP**HE**K**HY**L**H**	1
AcP**DY**K**HH**L**H**	1
AcP**HE**K**H**GL**H**	1
AcP**D**GK**HE**L**H**	1
AcP**D**RK**HH**L**H**	1
AcP**D**GK**HH**L**H**	1

Table S2. Occurrence of the peptides selected during the activity-based assay. The GRPPβA-OH sequence at the C-terminal is omitted for clarity. The coordinating amino acids are shown in bold.

	Z-Position		
AA	2	3	6
H	4	**4**	**8**
E	0	**10**	**7**
D	**14**	0	0
R	0	2	0
Y	0	1	2
G	2	3	3

Table S3. Analysis of the amino acids found at the variable positions (Z) in sequence $AcP_1Z_2Z_3K_4H_5Z_6L_7H_8$. The GRPPβA-OH sequence at the C-terminal is omitted for clarity.

Position	α		β		γ		δ		ε		ς	Other signals
amino acid	δ_H	δ_C	δ_H	δ_C	δ_H	δ_C	δ_H	δ_C	δ_H	δ_C	δ_H	
Ac												2.02 (CH_3) 21.39/21.58 (CH_3)
P	4.25	60.1	1.76/2.15(trans) 2.32/3.55(cis)	29.9 31.7	1.29 1.87	24.1 24.3	3.55	48.8				
D	4.48	51.4	2.55	38.3								117.35 (CO(OH)) 8.32 (NH)
H	4.5	53.7 54.1	3.09	28.1 28.4		132.5	6.92-7.02	117.2	7.91-7.99	136.0		7.9-8.0 (NH)
K	4.12	53.4	1.57	26.3	1.20	22.0	1.57	29.9	2.88	39.5	7.40	8.10 (NH)
H	4.5	53.7-54.1	3.01	28.1 28.4		132.5	6.92-7.02	117.2	7.91-7.99	136.0		7.9-8.0 (NH)
H	4.5	53.7 54.1	3.01	28.1 28.4		132.5	6.92-7.02	117.2	7.91-7.99	136.0		7.9-8.0 (NH)
L		52.7	1.40	39.5	1.32			20.7 22.3	0.76			8.16 (NH)
H	4.5	53.7 54.1	2.96	28.1 28.4		132.5	6.92-7.02	117.2	7.91-7.99	136.0		7.9-8.0 (NH)
NH_2 carboxamide												7.05

Table S4. Assignment of the ^{1}H and ^{13}C chemical shifts of OCP1.

1. Supplementary figures

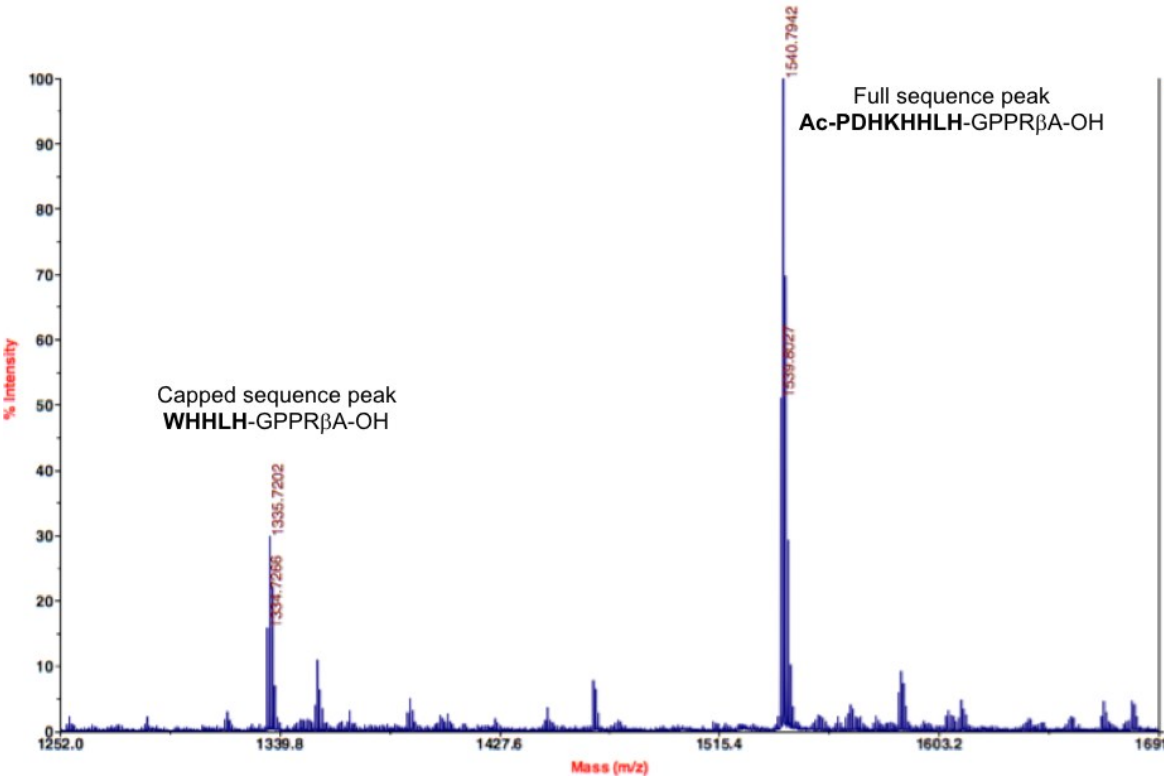

Figure S1. Typical mass spectrum of a cleaved bead and attribution of the peaks of the peptide fingerprint. The residues written in bold correspond to part of the sequence tested for coordination and activity. The others have been introduced to increase the mass of the sequence.

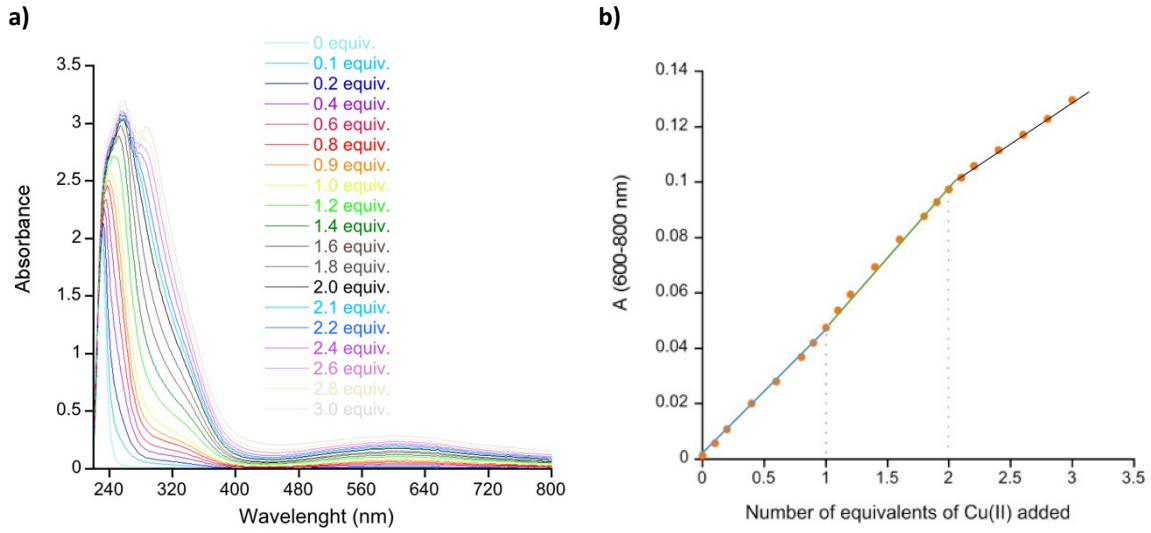

Figure S2. UV-visible titration of OCP1 (1 mM) with increasing amounts of Cu^{2+} at 25°C. a) The spectra were recorded in HEPES (50 mM, pH 7.5). b) The absorbance at 600 nm (in the d-d bands area) was corrected with the absorbance at 800 nm to remove the diffusion contribution to the signal.

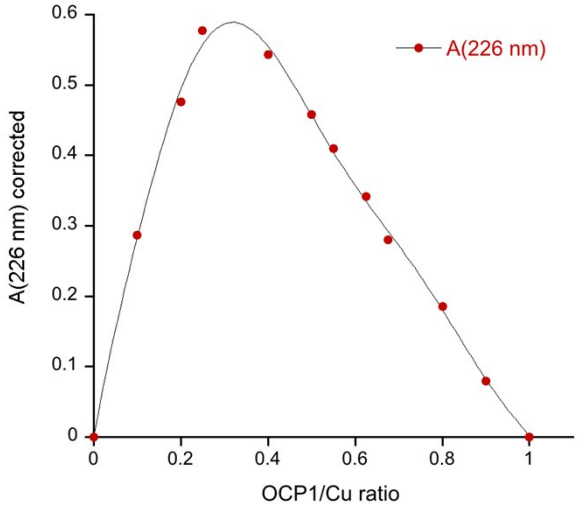

Figure S3. Job plot of OCP1-Cu complex performed in HEPES buffer (50 mM, pH 7.5) by UV at 25°C. Different ratios of Cu^{2+} and OCP1 were mixed to reach a total concentration of 200 µM. The absorbance was measured at 226 nm and corrected by subtracting the contribution of the copper and peptide alone.

$Cu_pH_qL_r$	log⍰	p*K*
CuH_3L	29.37(2)	4.38
CuH_2L	24.99(1)	5.47
CuHL	19.52(2)	7.38
CuL	12.14(4)	7.55
$CuH_{-1}L$	4.59(3)	9.05
$CuH_{-2}L$	-4.46(3)	10.34
$CuH_{-3}L$	-14.80(4)	
$Cu_2H_{-1}L$	11.22(2)	7.13
$Cu_2H_{-2}L$	4.09(4)	7.28
$Cu_2H_{-3}L$	-3.19(3)	9.18
$Cu_2H_{-4}L$	-12.37(3)	10.38
$Cu_2H_{-5}L$	-22.75(4)	10.82
$Cu_2H_{-6}L$	-33.57(3)	

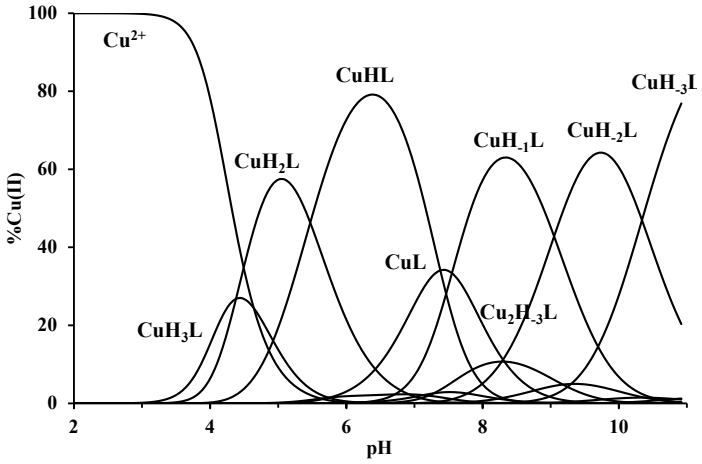

Figure S4. *Left*: Formation constants (log*β*) and derived data (p*K*) of the Cu^{2+}–OCP1 complexes (the estimated errors in the last digit are in parentheses), *I* = 0.1 M NaCl, *T* = 298 K. Formation constants (logβ) of the free ligand OCP1 (as $[H_nL]^{(n-1)+}$ species, n=6,5,4,3,2,1) are as follows: 37.84(4), 34.91(3), 29.77(3), 23.69(3), 17.38(3) and 10.29(1). *Right*: Distribution of the species in the Cu^{2+}–OCP1 1:1 system ($[OCP1]_{tot} = [Cu^{2+}]_{tot}$ = 0.001 M, *I* = 0.1 M NaCl, and *T* = 298 K). Charges of the complexes are omitted for clarity.

The peptide OCP1 has five accessible metal-coordinating group side chains: 4 imidazole groups and 1 carboxylate group. The lysine ε-amino group, which is generally not a coordinating group, remains protonated throughout the studied pH range (its p*K* in the free ligand is 10.29). The p*K*s of formation of CuH_2L and CuHL complexes ($CuH_3L = CuH_2L + H^+$, p*K* = 4.38, and $CuH_2L = CuHL + H^+$, p*K* = 5.47) are lower than the p*K*s of the imidazole rings in the free ligand, showing their involvement in the binding of metal ion. The low intensity of the CD spectra (Figures S4, S5) in the UV and also in the visible region at acidic pH (<5) indicate similarly the coordination of only side chain donor atoms in these complexes. Considering the protonation states of the mentioned species and the number of histidines in the sequence, the coordination of $2N_{im}$ and $3N_{im}$ can be suggested in CuH_3L and CuH_2L complexes respectively, probably in the form of different coordination/protonation isomers, where the

coordination sphere might be completed by the carboxylate group or water molecule(s). In the following species formed in equimolar solution, the subsequent deprotonations are related to metal-induced proton loss and coordination of amide nitrogens (N^-).

The continuous blue shift of the Cu^{2+} d-d band on the visible absorption spectra and the appearing negative CD band in the UV region from pH 5.8 (Figures S4, S5) support one to three amide nitrogens coordination in the CuHL – $CuH_{-2}L$ series. Based on these spectral changes and the protonation state, it can be suggested that CuHL complex possesses a $\{3N_{im},N^-\}$ coordination sphere with a protonated lysine ε-NH_3^+ and one imH^+ group. The following deprotonation steps of CuHL and CuL species significantly overlap (p*K* = 7.38 and 7.55, respectively) suggesting the occurrence of alternative microdeprotonations. Thus, the deprotonation of CuHL complex ($\{3N_{im},N^-\}$+imH^+,ε-NH_3^+) can lead to the formation of two tautomeric forms by the deprotonation of either the amide group ($\{2N_{im},2N^-\}$+imH^+,ε-NH_3^+) or the uncoordinated imidazole ring ($\{3N_{im},N^-\}$+im,ε-NH_3^+). The latter species is itself a mixture of two tautomeric forms depending on whether the deprotonation of the imidazolium cation occurs on the N3 or N1 nitrogens. The subsequent deprotonation step from all these tautomeric forms results in the $CuH_{-1}L$ complex with ($\{2N_{im},2N^-\}$+im,ε-NH_3^+) protonation state. To note, the deprotonation of amide nitrogen prior to imidazole deprotonation and coordination is supported by the simulation of OCP1-Cu 1:1 complex structure using Spartan 16 software that did not give stable structure with $4N_{im}$ coming from the same ligand and bound to Cu^{2+}. The additional "extra" amide deprotonation takes place in the $CuH_{-2}L$ species leading to the coordination sphere $\{N_{im},3N^-\}$ around the metal ion. The last deprotonation corresponds to the loss of proton on lysine ε-NH_3^+. It should be mentioned that peptides bearing -HXH- sequences usually form highly stable $\{N_{im},N^-,N^-,N_{im}\}$ type complexes[9], due to the thermodynamically favoured, coupled chelate ring system (7,5,6) and even more stable complexes for $\{N_{im},3N^-\}$coordination implying a (5,5,6)[10] membered chelate similar to ATCUN motives.[11,12,13] The OCP1 peptide contains two of this motif, probably causing isomerism in these complexes. In summary, at physiological pH and at 1 mM, three species: CuHL, CuL, $CuH_{-1}L$ are mainly formed. When the distribution diagram is recalculated at 100 nM, according to the constants found, the same three species are still predominant with about 33% of each (Figure S7).

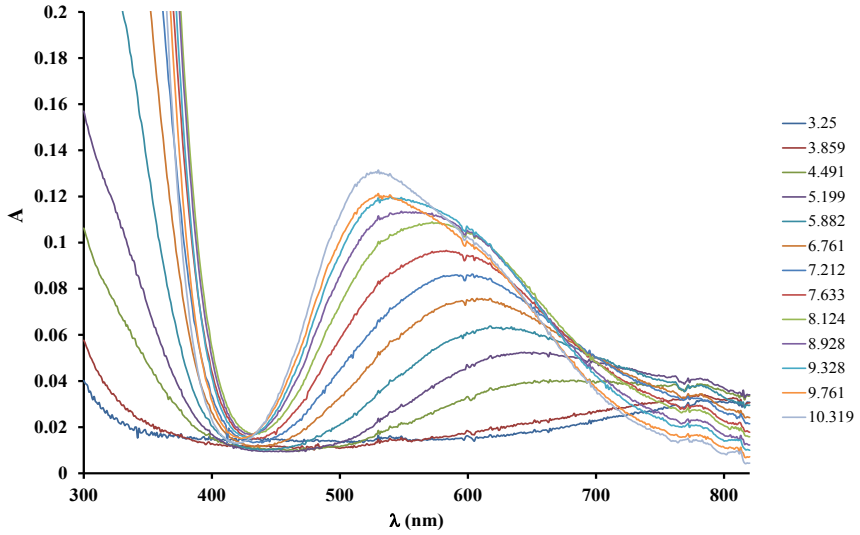

Figure S5. UV-vis absorption spectra of the OCP1- Cu^{2+} 1:1 system upon change of solution pH. [OCP1] = [Cu^{2+}] = 1.2×10^{-3} M.

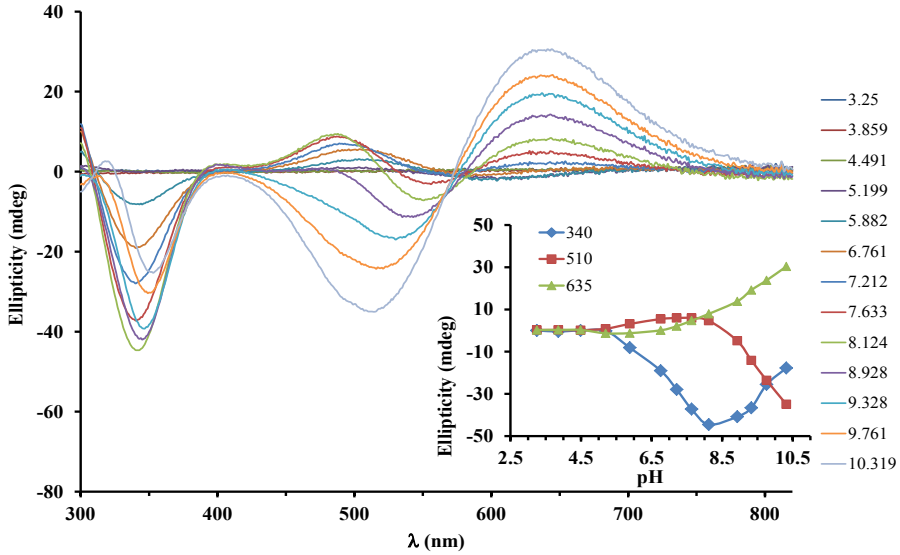

Figure S6. CD spectra of the OCP1- Cu^{2+} 1:1 system upon change of solution pH. [OCP1] = [Cu^{2+}] = 1.2×10^{-3} M. Insert: Variation of CD intensities at 340, 510 and 635 nm in function of pH.

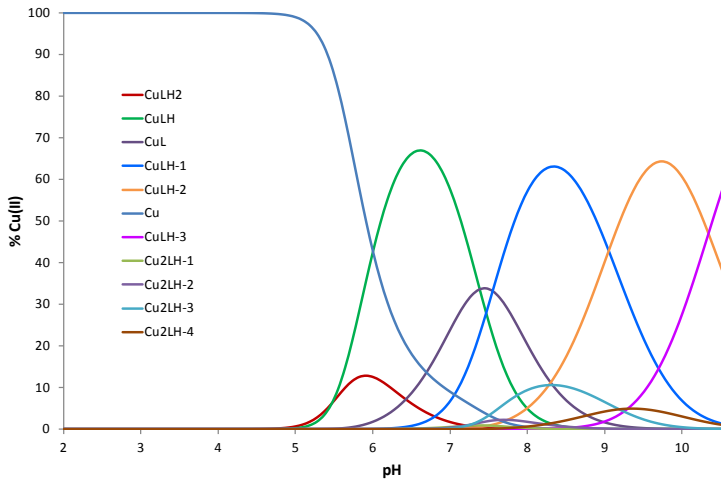

Figure S7. Recalculated distribution of the species in the Cu^{2+}–OCP1 1:1 system at 100 nM. Charges of the complexes are omitted for clarity.

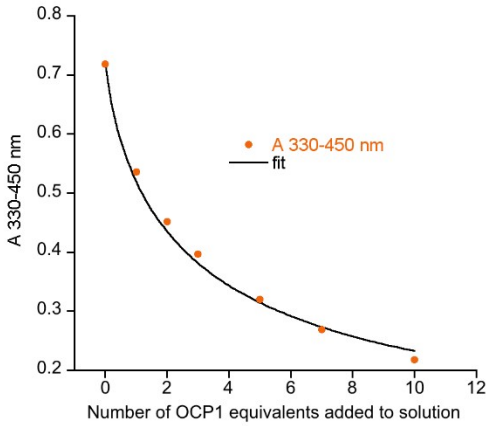

Figure S8. Example of a fit for the determination of the apparent dissociation constant of OCP1- Cu^{2+}in HEPES 50 mM pH 7.5.

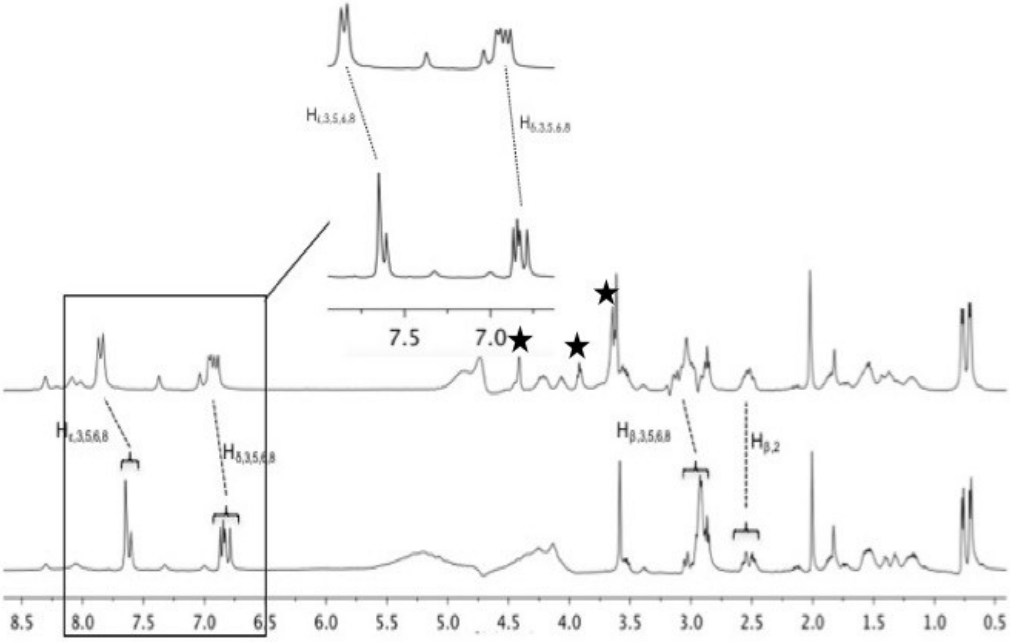

Figure S9. ^{1}H NMR spectra of 10 mM OCP1 peptide in Tris-d_6 buffer (300 mM pH 7.5) (bottom spectrum) and in presence of 0.9 equiv. of Cu^{+}, 1.5 equiv. of sodium ascorbate (top spectrum). *T* = 298 K, ν = 600 MHz. The spectra are barely the same except for the signals corresponding to the H_{ε} and H_{δ} of the four histidine residues that are slightly shifted in the presence of Cu^{+}. Stars show peaks attributed to sodium ascorbate.

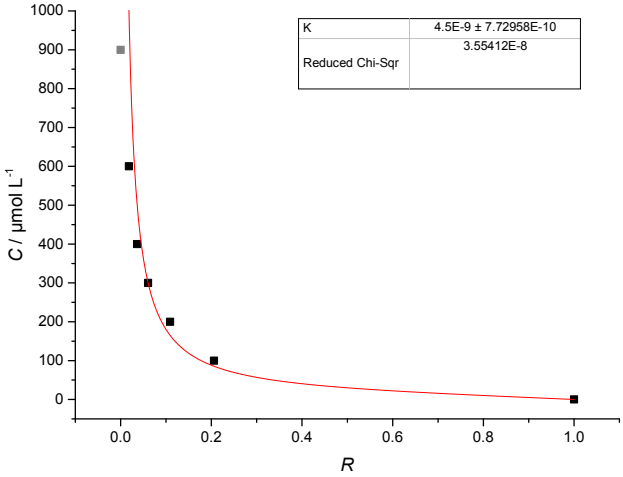

Figure S10. Example of a fit for the determination of the apparent dissociation constant of OCP1-Cu^{+} in HEPES 50 mM pH 7.5. The K_{Dapp} value given is the average of three independent measures.

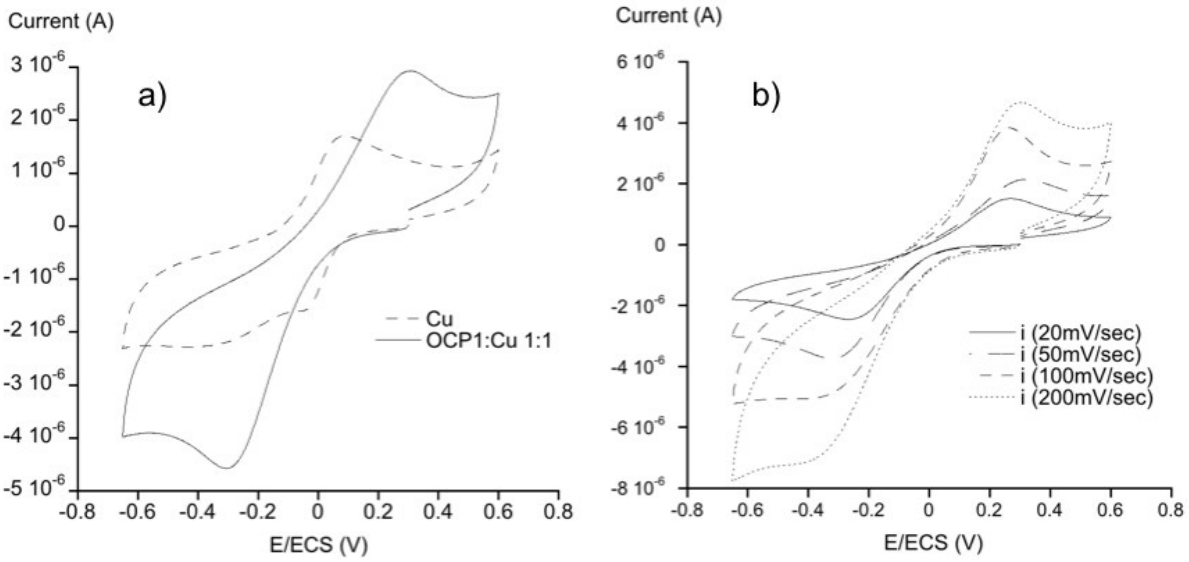

Figure S11. Cyclic voltammetry of the complex OCP1- Cu^{2+}. a) Voltamogram of Cu^{2+} (1 mM) and a OCP1- Cu^{2+} mixture with a 1:1 ratio (1 mM) in HEPES buffer (100 mM, pH 7.5) with a scan rate of 200 $mV.s^{-1}$. b) Influence of the scan rate on the redox potentials of the complex OCP1- Cu^{2+} 1:1 (1 mM) in HEPES (100 mM buffer, pH 7.5). Working electrode: Glassy carbon (3 mm diameter), counter electrode : Platinum, reference elctrode: SCE.

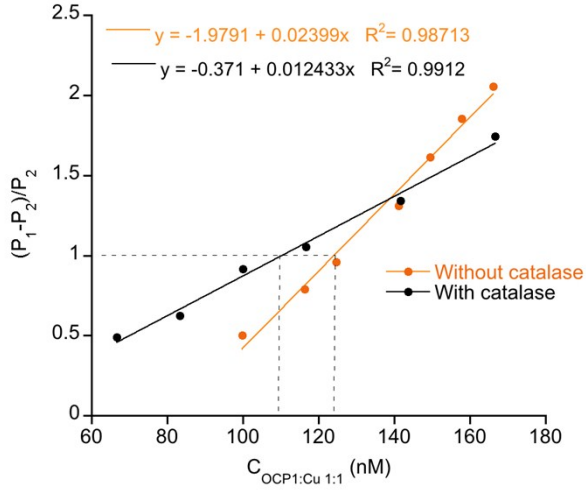

Figure S12. Fridovich assay for OCP1- Cu^{2+} 1: 1 with catalase (15 µg mL^{-1}) and without.

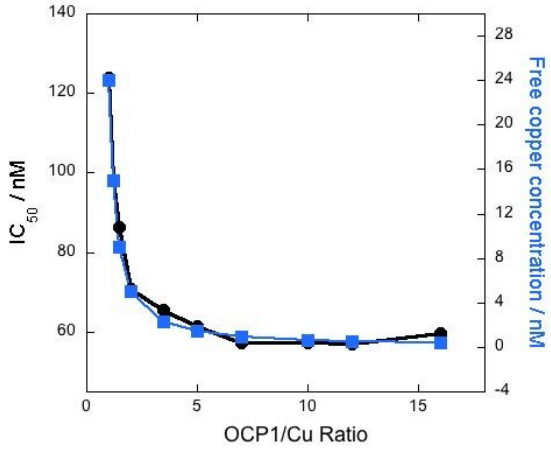

Figure S13. Evolution of IC_{50} (nM) (black circles) and free copper concentration (blue squares) according to the ratio OCP1:Cu^{2+} x:1.

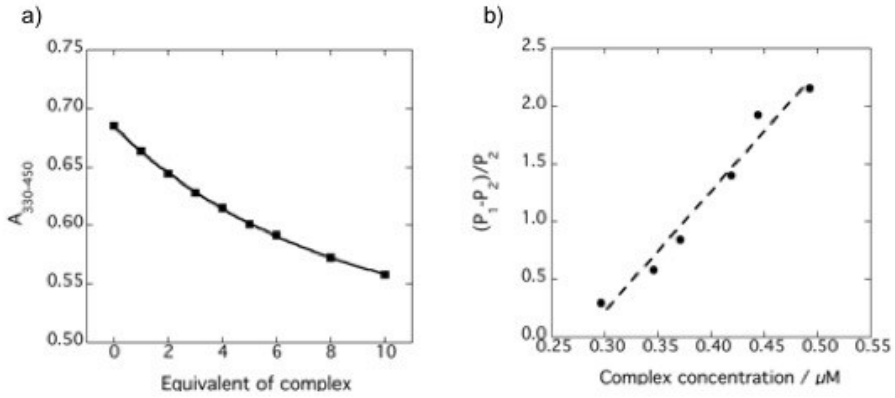

Figure S14. a) Example of a fit for the determination of the apparent dissociation constant of Ac-PHYKHRLH-NH_2-Cu^{2+} 1:1 complex by the competition assay using baba-Cu^{2+} in HEPES 50 mM pH 7.5. The K_{Dapp} value given is the average of 2 independent measures. b) Fridovich assay for PHYKHRLH-NH_2-Cu^{2+} 1: 1 in HEPES 50 mM, pH 7.5.

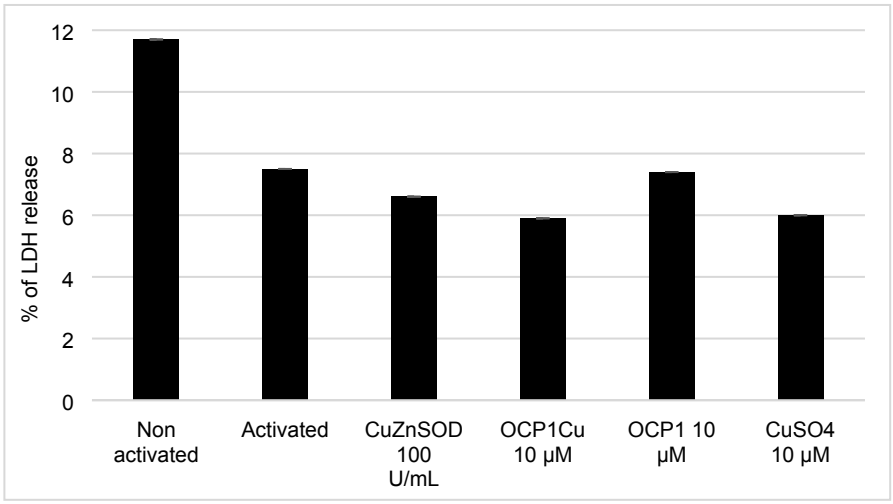

Figure S15. LDH assay on macrophages cells incubated with the native enzyme CuZnSOD, the peptidyl ligand, the metal salt and the corresponding copper complex at 10 µM. A value below 10 indicates that no significant cytotoxicity is observed.

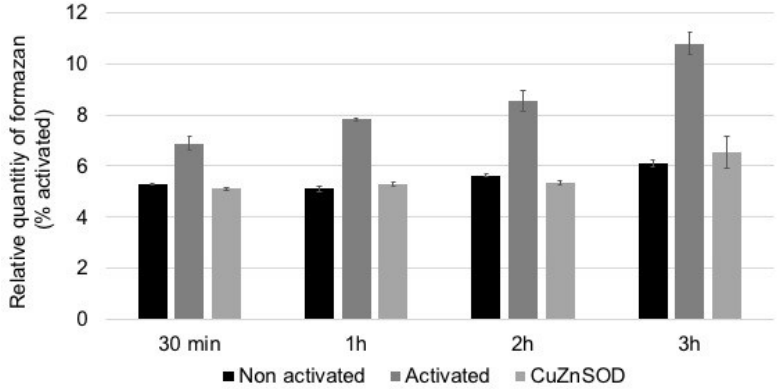

Figure S16. Kinetics of superoxide production by macrophages measured using XTT (200 µM). The grey bars correspond to the effect of the CuZnSOD (100 U/mL) incubated with the XTT.

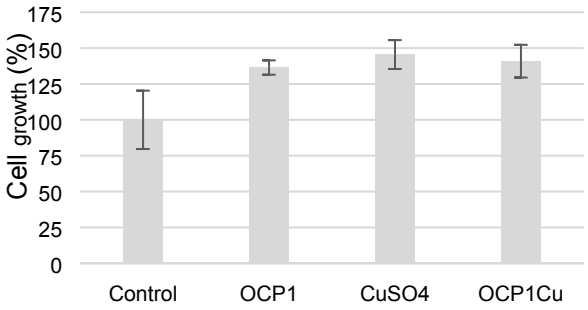

Figure S17. MTT assay on macrophages Raw 267.7 after incubation at 100 µM for 24 hours.

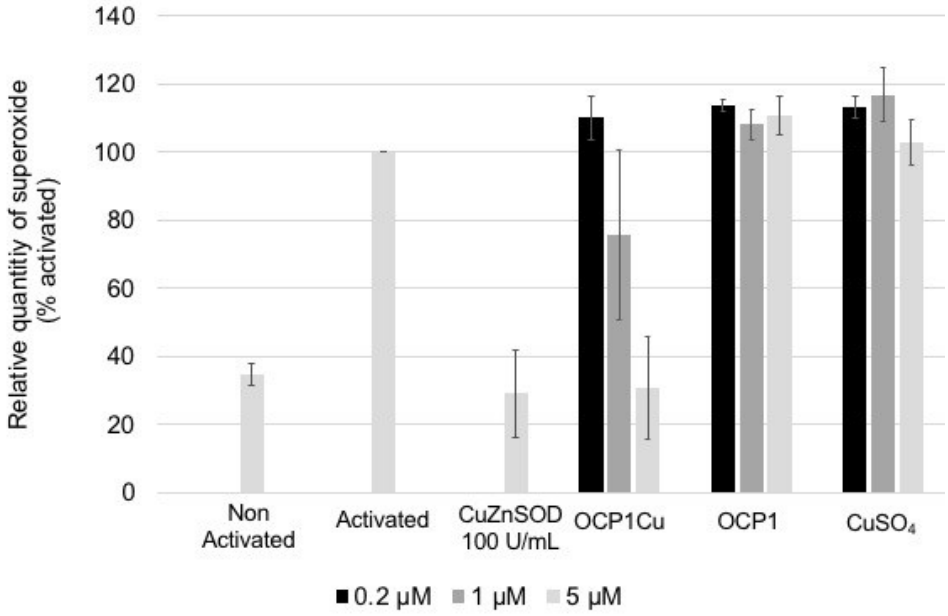

Figure S18. Superoxide dismutase activity on Raw 264.7 macrophages. The extracellular concentration of superoxide is measured by UV using cytochrome c as specific UV-vis marker (550 nm). The absorbance measured for activated cells was arbitrary set at 100%. Data represent mean ± SEM for two independent experiments

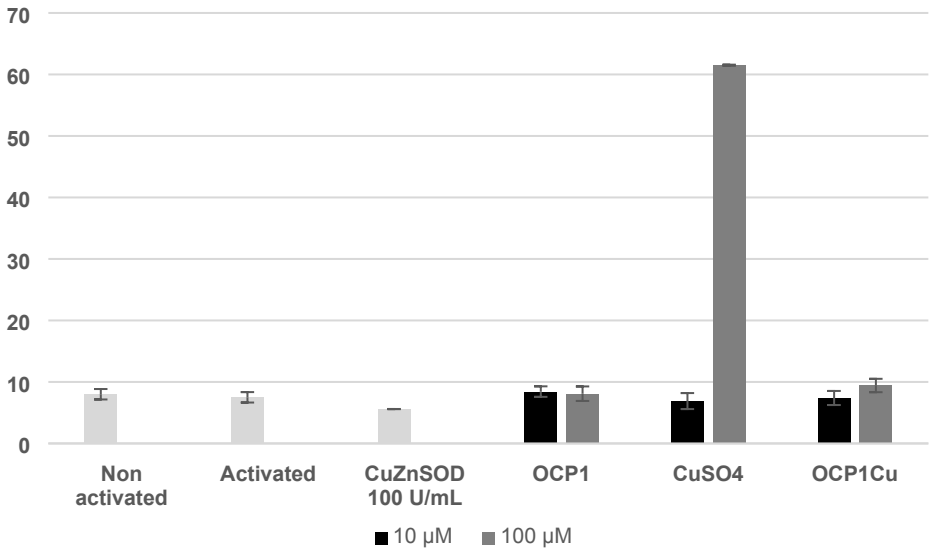

Figure S19. LDH assay on HT29-MD2 cells incubated with the native enzyme CuZnSOD, the peptidyl ligand, the metal salt and the corresponding copper complex at 10 and 100 µM. A value below 10 indicates that no significant cytotoxicity is observed.

2. Chemicals

All chemicals and solvents were of synthesis grade and were used as received without further purification. Common solvents for solid support synthesis and L-amino acids were obtained from either Sigma Aldrich, Novabiochem or Iris biotech GMBH.

3. Instruments

- HPLC: analytical HPLC was performed on an Agilent 1200 series equipped with a quaternary pump using a Proto 200 C18 from Higgins Analytical Inc (particles size 3 µm, 100×4.6 mm column). Preparative HLC was performed on an Agilent 1260 Infinity using a Nucleodur C18 HTech column from Macherey-Nagel Inc. (particles size 5 µm, 250×16 mm column).

- Mass spectrometry: MALDI-TOF mass spectrometry analysis of the peptide OCP1 and the complex OCP1/Cu:1/1 was performed in the positive ion reflector mode on Voyager DE-Pro MALDI-TOF mass spectrometer (Applied Biosystems) using as matrix a solution of α-Cyano-4-hydroxycinnamic acid (CHCA) at 10 mg/mL in CH_3CN:H_2O:CF_3COOH (50:50:0.2). Calibration was performed using external standards (Proteomix 4, LaserBio Labs Sofia-Antipolis, France).

- UV-vis spectrometry: UV−visible spectra were recorded on a CARY-5 UV−visible spectrophotometer using a double-beam mode with media as the reference or on a SPECORD S600 Analytik Jena spectrophotometer.

- Peptide synthesizer: Advanced ChemTech automated synthesizer

- NMR spectroscopy: the NMR experiments were performed at 298K on a Bruker model spectrometer with a proton frequency of 600 MHz equipped with a triple resonance inverse detection probe with triple axes pulsed field gradients.

- EPR spectroscopy: Elexsys E 500 Bruker spectrometer, operating at a microwave frequency of approximately 9.5 GHz. Spectra were recorded using a microwave power of 20 mW across a sweep width of 150 mT (centered at 310 mT) with modulation amplitude of 0.5 mT. Experiments were carried out at 110 K using a liquid nitrogen cryostat.

- Cyclic Voltammetry: MetrOhm potentiostat (AUTOLAB model). The auxiliary electrode was a Pt wire and the working electrode was a glassy carbon disk (3 mm diameter) carefully polished before each voltammogram with a 1 µm diamond paste, washed with water and finally air dried. The reference electrode was a SCE saturated with KCl.

4. Procedures

4.1. Library preparation

Identification of the peptide sequence by maldi mass spectrometry: capping strategy

As in all combinatorial libraries of peptides, isobaric sequences of peptides have been generated. In order to identify unambiguously the peptides by a simple MALDI mass spectrometry analysis, the strategy developed by Griesinger and coworkers and modified by Imperiali's group has been applied. Briefly, during the peptide

elongation, as soon as an isobaric sequence has been generated, a small portion of peptide (10%) has been capped using mass ladders that are Boc protected amino acids. Consequently, a truncated sequence with a known molecular weight has been generated at each position for which isobaric sequences are produced. At the end, for a given bead, the mass spectrum of the released peptide exhibits peaks corresponding to its molecular weight and to the molecular weights of the capped peptides. The combination of the mass peaks gives a "fingerprint" of the peptide that allowed its formal identification. To determine when isobaric sequence have been generated and thus the capping positions, the Biblio software developed by Griesinger and coworkers has been used.[14]

Synthesis: the peptide library on beads was prepared according to an already published procedure using a "split and mix" strategy leading to a one bead one peptide library.[15] Solid-phase peptide synthesis was performed manually using Fmoc chemistry on Tentagel macrobeads (0.24 mmol g^{-1}, 280-300 μm). Positions in the library that led to isobaric sequences and required capping to distinguish them were determined using the Biblio software.[16] Once capping positions were revealed, manual calculations determined which commercially available capping reagent combination would lead to a nondegenerate mass ladder. Mass caps used were Boc-Trp(Boc)-OH, Boc-Ile-OH, Boc-Ala-OH, Boc-Asn(Trt)-OH, Boc-Phe-OH. Where possible, the capping agent most similar to the amino acid that it encodes was used, for example, Ac-Ala-OH codes for Gly or Boc-Phe-OH codes for Tyr. As shown in Scheme S1 (SI), the resin was split into equal portions when variability is tested, one for each amino acid. Then, standard peptide coupling procedures were used for all single amino acid couplings, in which we treated amino acid (3 equiv/equiv resin) with benzatriazole-1-yl-oxy-tris-pyrrolidino-phosphonium hexafluorophosphate (HBTU, 3 equiv/equiv resin), 1-hydroxybenzotriazole (HOBT, 3 equiv/equiv resin), and diisopropylethylamine (DIPEA, 6 equiv/ equiv resin) in N-methyl-2-pyrrolidone (NMP) for 45 minutes at room temperature. The completion of the couplings was monitored using the Kaiser test that allows detecting free amines. In case of a positive result, the same amino acid was coupled again. Standard Fmoc deprotection conditions were employed (20% piperidine in NMP, 3 mL), once for 1 min and once 15 min at room temperature. Couplings with more than one free acid, that is, mass encoding steps and orthogonal linker coupling, involved treatment with N,N'-diisopropylcarbodiimide (DIC, 10 equiv/equiv acid) and N-hydroxybenotriazole (HOBt; 10 equiv/equiv acid) in NMP for 1 hour. Orthogonal linker coupling was achieved by coupling of 10-[(3-Hydroxy-4-methoxybenzylidene)]-9(10H)-anthracenone (HMBA) and 3-(Fmoc-amino)-3-(2- nitrophenyl)propionic acid (Fmoc-ANP) linkers (9: 1, total 5 equiv/equiv resin) to the peptide. The βAla residue directly coupled to the orthogonal linkers was introduced by treatment of the beads with the symmetrical anhydride of the residue (6 equiv/equiv resin) and 4-dimethylaminopyridine (4-DMAP) at room temperature. Encoded mass capping was achieved by coupling a mixture of the desired amino acid and mass cap (9: 1, 10 equiv/equiv resin) to the peptide. Final acetylation was performed by adding a solution of acetic anhydride in DCM (3 mL, 20/80 v: v) to the resin for 1h at room temperature. After filtration, the resin was washed extensively with DCM and then extensively with MeOH. The resin was dried under vacuum for 1h. Side chains were deprotected by treatment with 95 % trifluoroacetic acid (TFA), 2.5% H_2O, and 2.5% triisopropylsilane for 3h at room temperature. Resin was then

washed sequentially with TFA (10 mL), dichloromethane (5×10 mL), DMF (5×10 mL), and finally HEPES (100 mM, 3×10 mL; pH 7.4)

Complexes formation on beads: approximately 300 - 500 beads were suspended in a solution of $CuSO_4$ (50 mM) in HEPES (100 mM, 1 mL; pH 7.4) and allowed to equilibrate (1 hr) at room temperature. The solution was then removed by filtration. To increase the selective pressure on later generations of the library, after Cu^{2+} incubation and draining of the solution, beads were suspended in ethylenediaminetetraacetate (EDTA, 50 mM) for 1 minute before being washed three times with HEPES (100 mM, pH 7.4) so that only 5 to 10 beads with halos were visible in each gel screened.

4.2. Gel screening

The above treated beads were suspended into molten agarose (2 %) in HEPES (100 mM, pH 7.4), poured into a circular Petri dish, and allowed to cool to room temperature. The gel was soaked in a solution of NBT (2.43 mM), tetramethylethylenediamine TEMED (28 mM), riboflavin (28 mM) in deionized H2O (15 mL) for 20 min at room temperature. It was washed with H_2O ($\times$3) and then was placed on a mid-range UV transilluminator (UVP, high-performance transilluminator) for 3 minutes. Beads with yellow halos were cut from the agarose with a truncated tip and transferred to a 1.5 mL plastic tube. The residual agarose surrounding the bead was melted away in distilled H_2O (1 mL) at 110°C. The selected bead was subsequently washed with EDTA (50 mM, pH 8.0, 15 minutes, 100 µL), then extensively with H_2O (3 $\times$ 100 µL), and then covered with ammonium hydroxide (28 %, 50 µL) and left to incubate overnight at room temperature. After cleavage, the ammonium hydroxide was removed under vacuum and the peptide residue resuspended in deionized water (100 µL). The sequences of the peptides were determined by recording a MALDI-TOF mass spectrum. A portion of the peptide stock solution (1 µL) was mixed with a solution (1 µL, 5:5:0.01 CH3CN/H_2O/TFA) of α-cyano-4-hydroxycinnamic acid matrix (10 mg mL^{-1}). The resulting solution (1 µL) was deposited onto a MALDI plate and air dried. The Biblio software as well as manual calculations were used to determine the sequences of the peptides from the mass spectra (See for an example Figure S1).

4.3. Potentiometry

4.3.1. Procedure

The protonation and coordination equilibria were investigated by pH-potentiometric titrations in aqueous solutions (I = 0.1 M NaCl and T = 298.0 ± 0.1 K) under argon atmosphere. The titrations were performed using a PC controlled Titrando 809 (Metrohm) automatic burette and pH-meter. The Metrohm micro glass electrode (125 mm) was calibrated by the titration of hydrochloric acid and the data were fitted using the modified Nernst-equation:[17]

$$E = E_0 + K \cdot \log[\mathrm{H}^+] + J_{\mathrm{H}} \cdot [\mathrm{H}^+] + \frac{J_{\mathrm{OH}} \cdot K_{\mathrm{w}}}{[\mathrm{H}^+]}$$

where J_H and J_{OH} are the fitting parameters representing the acidic and alkaline error of the glass electrode, respectively (Kw = 10-13.75 is the autoprotolysis constant of water[18]). The parameters were calculated by the non-linear least squares method. The formation of the complexes was characterized by the general equilibrium process:

$$pM + qH + rL \overset{\beta_{M_pH_qL_r}}{\rightleftharpoons} M_pH_qL_r$$

$$\beta_{M_pH_qL_r} = \frac{[M_pH_qL_r]}{[M]^p[H]^q[L]^r}$$

where M denotes the metal ion and L the fully deprotonated ligand molecule. Charges are omitted for simplicity, but can be easily calculated considering the composition of the protonated ligand at pH 2 ($[H_6L]^{5+}$). The protonation constants of the ligand and the formation constants of the complexes were calculated by the PSEQUAD computer program[19] from 5, and 7 independent titrations respectively (ca. 90 data points per titration). The metal ion concentrations varied between 1.3-2.2×10^{-3} M, using 2:1 and 1:1 metal-to-ligand ratios.

4.3.2. Data analysis

4.4. Apparent association constant determination by competition using UV-visible spectrometry

4.4.1. Competition experiment with Copper(II):

To determine the apparent association constant of OCP1-Cu^{2+}, the procedure described by Hureau et coll. using 4-bis(oxamato)benzoic acid ligand (Baba) was followed.[20] In brief, the Cu-Baba complex, that presents a strong and specific signature in UV-vis was formed in HEPES buffer (0.1 M, pH = 7.5) and its disappearance was followed by UV-vis spectrometry upon successive additions of OCP1.

The ligand Baba (50 µM in theory) and Cu^{2+} (45 µM in theory to avoid any free copper in solution) were mixed in 3 mL quartz cuvettes and OCP1 was sequentially added to reach a concentration of 500 µM. Each addition of the peptide was made once the thermodynamic equilibrium of the previous reaction was reached. The competition experiments were performed at 25°C in triplicate. The data were analyzed following a 2-step procedure. First, the theoretical concentrations of the ligand Baba and the Cu^{2+} were adjusted using the absorbance of ligand at 246 nm ($\varepsilon_{246} - \varepsilon_{450}$ = 18000 $cm^{-1}.M^{-1}$) and the absorbance of the Cu(Baba) complex at 330 nm ($\varepsilon_{330} - \varepsilon_{450}$ = 18000 $cm^{-1}.M^{-1}$) respectively. Then, the absorbance measured at 330 nm at the equilibrium was plotted as a function of the number of peptide OCP1 equivalents recalculated with respect to the experimental Baba concentration. Then these data were fitted with an in-house procedure using the adjusted concentrations as starting parameters and the following epsilons:

OCP1 $\varepsilon_{330} - \varepsilon_{450}$ = 0 $cm^{-1}.M^{-1}$

OCP1-Cu $\varepsilon_{330} - \varepsilon_{450}$ = 510 +/- 50 $cm^{-1}.M^{-1}$

The epsilon of OCP1-Cu^{2+} was not determined very precisely as it does not influence in a large extent the fit because of its low value.

Two equilibriums are considered:

"Cu^{2+}" is written in a simple manner but it is probably coordinated to an unknown quantity of water and HEPES molecules. The dissociation constant calculated is apparent (HEPES 50 mM, pH 7.5). The value might be different

in other buffers and ionic strengths.

OCP1 + Cu(II) = OCP1-Cu		
C_0	C_1	0
C_0 - x	C_1 – x – x’	x

Baba + Cu(II) = Baba-Cu		
C_2	C_1	0
C_2 – x’	C_1 – x – x’	x’

$$\frac{K_d^{OCP1-Cu}}{K_d^{Baba-Cu}} = \frac{[OCP1][Cu(II)]\ \ [Baba-Cu]}{[OCP1-Cu]\ \ [Cu(II)][Baba]}$$

Regarding C_0,C_1 and C_2 and the rather high affinity constant for both OCP1-Cu and Baba-Cu, Cu(II) is supposed to be chelated by the peptide OCP1 or by Baba. There is no free Cu(II). As a consequence, the equation can be simplified like that:

$$\frac{K_d^{OCP1-Cu}}{K_d^{Baba-Cu}} = \frac{(C_0 - x)\quad (C_1 - x)}{x\quad (C_2 - C_1 + x)}$$

Which gives the second-degree equation to solve: $ax^2 + bx + c = 0$

With

$$a = \frac{K_d^{OCP1-Cu}}{K_d^{Baba-Cu}} - 1$$

$$b = \frac{K_d^{OCP1-Cu}}{K_d^{Baba-Cu}}(C_2 - C_1) + C_0 + C_1$$

$$c = -C_0.C_1$$

$$x = \frac{-b + \sqrt{\Delta}}{2a}$$

And $A_{330\text{-}450nm} = \varepsilon_{Baba\text{-}Cu(330\text{-}450)}(C_1\text{-}x) + \varepsilon_{Baba(330\text{-}450)}(C_2\text{-}C_1\text{+}x) + \varepsilon_{OCP1\text{-}Cu(330\text{-}450)}*x + \varepsilon_{OCP1(330\text{-}450)}*(C_0\text{-}x)$

An example of fit is in Figure S8.

4.4.2. Competition experiment with Copper(I):

To determine the apparent association constant OCP1-Cu^+, the procedure described by Hureau et coll. using ferrozine was followed.[21] The complex $[Cu(Fz)_2]^{3-}$ presents a strong and specific signature in UV-vis in HEPES buffer (0.1 M, pH = 7.5). Its disappearance was followed by UV-vis spectrometry upon successive additions of OCP1.

The ligand Ferrozine (105 µM in theory) and Cu^{2+} (50 µM in theory to avoid any free copper in solution) were mixed in 1 mL quartz cuvettes previously degassed under argon for 5 minutes. Ascorbate (previously dissolved in degassed milliQ water) is then added to the cuvette to reach a concentration of 100 µM. OCP1 was then sequentially added to reach a concentration of 900 µM. Each addition of the peptide was made once the thermodynamic equilibrium of the previous reaction was reached. At the end of the experiment, ascorbate was added again to ensure that no oxidation of Cu^+ happened, which would modify the absorbance and the value of the constant. The competition experiments were performed at 25°C in quadruplicate. The apparent constant found for Cu^+ and OCP1 is $6.0 \pm 0.4.10^{-9}$ (Figure S10).

Calculations: The data were analyzed using the following equilibriums and equations:

OCP1 + Cu(I) = OCP1-Cu(I)		
C_2	C_0	0
C_2 - x	C_0 – x – x’	x

2Fz + Cu(I) = $[Cu(I)(Fz)_2]^{3-}$		
C_1	C_0	0
C_1 – 2x’	C_0 – x – x’	x’

$$\frac{K_d^{OCP1-Cu}}{1/\beta_2} = \frac{[OCP1][Cu(I)] \quad [CuFz2]}{[OCP1-Cu] \quad [Cu(I)][Fz]^2}$$

$$\frac{K_d^{OCP1-Cu}}{1/\beta_2} = \frac{(C_2 - C_0 + x') \quad x'}{(C_0 - x') \quad (C_1 - 2x')^2}$$

Which can also be written this way since $x' = RC_0$, with R = $\frac{A - A_\infty}{A_0 - A_\infty}$

$$K_d^{OCP1-Cu} = \frac{1 \quad R}{\beta_2(1-R)C_0}\left[\frac{\frac{C_2}{C_0} - 1 + R}{\left(\frac{C_1}{C_0} - 2R\right)^2}\right]$$

A is the absorbance measured at 470 nm during the experiment

A_0 is the absorbance at 470 nm with 105 µM ferrozine, 50 µM copper and 100 µM ascorbate in solution

A_∞ is the absorbance at 470 nm after adding an infinite amount of peptide OCP1

A_∞ is let as a variable parameter

$1/\beta_2$ = 2.7 10^{-12} (in HEPES 100 mM, pH 7.4) according to literature[21]

4.5. NMR

NMR experiments were performed at 298 K on a spectrometer with a proton frequency of 600 MHz. The solvent was H_2O, while for the lock of the field a separate capillary filled with deuterated DMSO was inserted into the sample. Homonuclear TOCSY[22], NOESY[23] and ROESY[24] experiments were performed on the different samples using excitation sculpting[25] to suppress the water signal. For each of these experiments, the spectral width was 11 ppm in both dimensions and 1024×1024 complex points were acquired. In addition, heteronuclear single quantum (HSQC[26]) and multiple bond (HMBC[27]) correlation spectra were recorded. For the HSQC the spectral width was of 16 ppm × 160 ppm in the direct (^{1}H) and indirect dimension (^{13}C) for 1024 × 512 complex points. While for the HMBC the spectral width was 16 ppm × 220 ppm for 4096 × 512 complex points. All the ^{1}H and ^{13}C signals were assigned on the basis of chemical shifts, spin-spin coupling constants, splitting patterns and signal intensities, and by using ^{1}H-^{1}H TOCSY, ^{1}H-^{13}C HSQC and ^{1}H-^{13}C HMBC experiments.

4.6. In vitro SOD activity using the Mc Cord and Fridovich assay

4.6.1. Procedure

In the Fridovich assay, superoxide was generated with the xanthine/xanthine oxidase system. XTT was used as UV-Vis marker as it reacts with superoxide with a k = 2.9 ± 0.1 10^4 $M^{-1}s^{-1}$ (see next part for k_{XTT} determination) to give a formazan derivative that possesses a maximum of absorption at 470 nm. The kinetic measurements were consequently conducted at 470 nm using the following procedure: to a solution of xanthine (200 μM) and XTT (100 μM) in HEPES (50 mM, pH 7.4), a solution of xanthine oxidase (20 mg mL^{-1}) was added. The solution was quickly mixed and the measurement of the absorbance started (giving a first slope P1). The volume of xanthine oxidase solution was chosen according to the value of the slope P_1 of formazan formation that must be kept between 0.0025 and 0.0030 min^{-1}.[28] After 1.5 min, the compound of interest was added to the cuvette, the solution was mixed and formazan formation was measured between 2.5 and 4 min (slope P_2). The experiment was repeated for various concentration of the compound giving a set of collinear points, when plotting the ratio $(P_1-P_2)/P_2$ versus the concentration of the compound in the cuvette. The IC_{50} value corresponds to the complex concentration at $P_2 = P_1/2$, meaning half of the activity of the xanthine oxidase has been inhibited.

4.6.2. Determination of k_{XTT} and k_{McF}

The IC_{50} values measured depend on the UV marker used (XTT, Cytochrome c or NBT). In order to compare the efficiency of our catalyst to others complexes described in the literature, the kinetic constant k_{MCF}, which is independent of these markers, has been calculated.

This constant can be calculated with the following equation at the IC_{50}:

$$k_{MCF} * IC_{50} = k_{marker} * [marker]$$

In our case:

$$k_{MCF} * IC_{50} = k_{XTT} * [XTT]$$

That is to say,

$$k_{MCF} = \frac{k_{XTT} * [XTT]}{IC_{50}}$$

k_{XTT} can only be found in literature[29] under very specific conditions (phosphate buffer, 50 mM, pH 7.8). We have thus estimated the value of k_{XTT} in the conditions used in this study (HEPES 50 mM, pH 7.4). The catalytic constant of a studied complex Mn1 developed in Policar's group[30] has been found through a different technique (stopped-flow) and in very close conditions (HEPES 60 mM, pH 7.4). The value has been estimated at 5.0 ± 0.1 10^6 $M^{-1}s^{-1}$.

Knowing that:

$$\frac{P_1}{P_2} = 1 + \frac{k_{Mn1} * [Mn1]}{k_{XTT} * [XTT]}$$

By plotting $\frac{P_1}{P_2}$ in function of $[Mn1]$, k_{XTT} can be found (Figure S20).

The following procedure has been performed to calculate k_{XTT}:

Again, a solution of xanthine (200 μM) and XTT sodium salt (100 μM) in HEPES (50 mM pH 7.4) was used. The kinetics measurements were also conducted at 470 nm at 25°C. To 1.5 mL of the above-mentioned solution introduced into a UV-vis cuvette, a 20 mg/mL solution of xanthine oxidase (dissolved in milliQ water) was added.

The solution was quickly mixed and the measurement of the absorbance started. The volume of xanthine oxidase solution was chosen according to the value of the slope P1 of formazan formation that must be kept between 0.025 and 0.030 min^{-1}. After 1.5 min, Mn1 was added to the cuvette at different concentrations (0.1 µM to 4 µM), the solution was mixed and the slope P2 of formazan formation was measured between 2.5 and 4 min.

The experiment has been repeated three times, each time a new stock solution of Mn1 has been used and XTT has been reweighed.

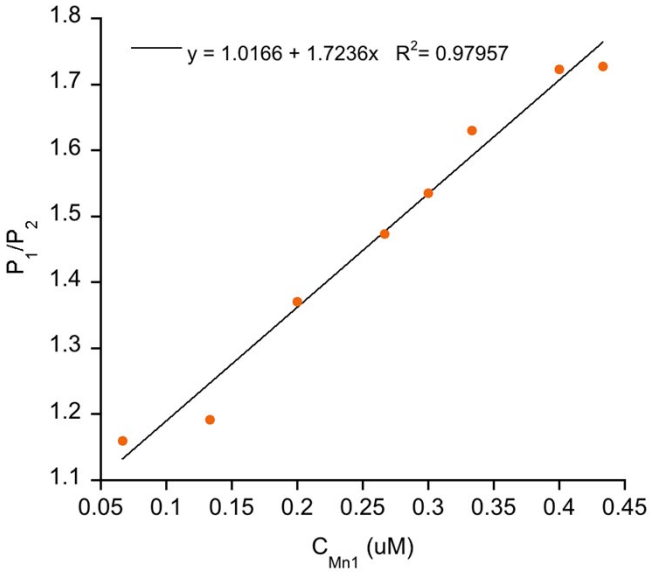

Figure S20. Plot of $\frac{P_1}{P_2}$ in function of $[Mn1]$ in HEPES (50 mM pH 7.4) at 25°C.

The k_{XTT} found is thus $2.9 \pm 0.1\ 10^4\ M^{-1}s^{-1}$. This value is almost 3 times smaller than the published one's ($8.6 \pm 0.8\ 10^4\ M^{-1}s^{-1}$) measured in phosphate buffer (50 mM, pH 7.8)[29] highlighting that it is mandatory to determine this constant in the experiment conditions to get accurate and comparable results.

6.6.3 Controls

It has been controlled that the intrinsic xanthine oxidase activity was not affected upon addition of the complexes and copper by monitoring the urate formation at 290 nm. It has also been controlled that the complexes do not modify the formazan absorption at 470 nm.

4.7. SOD activity measurement on macrophages

Cell culture. Murine macrophage RAW 264.7 (American Type Culture Collection) cell line was cultured at 37°C under a 5 % CO_2 atmosphere in Dulbecco's modified Eagle's medium (DMEM) containing 1.0 g L^{-1} D-glucose and sodium pyruvate (Invitrogen). The medium was supplemented with 5% fetal bovine serum (Invitrogen) and 20 µg mL^{-1} gentamicin (Sigma).

Cytotoxicity measured using the LDH assay. Cytotoxicity of the compounds (OCP1Cu and controls) was tested by following the release of the cytosolic lactate dehydrogenase (LDH) into the supernatant, indicating membrane damages, with a limit for non-cytotoxicity chosen at 10%. No cytotoxicity was observed in activated cells. The

assay is based on the ability of LDH contained in cell lysates or supernatants to catalyze the reduction of pyruvate (0.6 mM) into lactate in the presence of NADH (0.18 mM), which is oxidized to form NAD+ in PBS. The level of LDH was proportional to amount of pyruvate consumed measured by monitoring the decrease in absorbance (340 nm) due to oxidation of NADH during 1 min. The percentage of LDH release in supernatants was calculated by dividing this LDH activity found in supernatant, by the sum of activity in supernatants and cell lysates.

SOD activity measurement using XTT. XTT was used to assess the superoxide ion production in RAW 264.7 cells and evaluate their metabolic activity linked to oxidative stress. Cells were stimulated in a 24-well plate with culture medium (DMEM, 20 % SVFd, 1 % glutamin) containing 1 $U.mL^{-1}$ IFN- γ and 1 $ng.mL^{-1}$ LPS for 24 h at 37°C (except for the control). They were then incubated for 1h at 37°C in 0.1 M HEPES with XTT (200 µM), antioxidants (1 µM, 10 µM OCP1-Cu 1:1 or 100 $U.mL^{-1}$ SOD) and PMA (800 nM) (except for the control). After one hour, 200 µL of supernatant were collected and transferred into a 96-well plate for absorbance reading at 470 nm. Data are a mean ± SEM of five independent experiments.

Cytotoxicity measured using MTT assay. Cell growth and viability was assessed by the mitochondrial-dependent reduction of MTT (3-(4,5-dimethylthiazol-2-yl)-2,5-diphenyltetrazolium bromide) to formazan as previously reported.[31] After 24 hours of incubation without or with 250 µM complex OCP1-Cu 1:1 /ligand OCP1/$CuSO_4$, the macrophage cultures in the Petri dishes were incubated at 37°C with MTT (0.5 mg mL^{-1}) for 24 h. Culture medium was removed by aspiration and the cells were solubilized in 0.04 M HCl in absolute ethanol. The extent of reduction of MTT to formazan by the cells was quantified by the measurement of OD at 550 nm. The results are arbitrarily normalized to control samples and evidenced that incubations of the different compounds are not toxic in the conditions tested.

SOD activity measurement using ferricytochrome C. Ferricytochrome c reduction was used to assess the superoxide ion production in RAW 264.7 cells. Cells were seeded in a six-well plate to reach 90% of confluency after 3 days. They were stimulated with culture medium containing 1 U mL^{-1} IFN- γ and 1 ng mL^{-1} LPS for 24 h at 37°C (except for the control). They were then incubated 1h at 37°C with 1 mL of a medium (containing 14.6 mM glucose, 358 mM NaCl, 12.7 mM KCl, 3.1 mM KH_2PO_4, 6.1 mM $MgSO_4$, 3.1 mM $CaCl_2$, 13 mM $NaHCO_3$ in HEPES buffer (53 mM pH 7.4)) with 100 µM ferricytochrome c, with or without antioxidant (0.2 µM, 1 µM, 5 µM OCP1-Cu 1:1 or 100 U mL^{-1} SOD) and with 800 nM PMA. The absorbance of supernatants was read at 550 nm with a Cary 300 Bio Spectrophotometer. Data are a mean ± SEM of two independent experiments. For each experiment, the different conditions were tested in duplicate.

4.8. Anti-inflammatory activity on HT29-MD2 cells

Cell culture. HT29 human colon adenocarcinoma were obtained from the European Collection of Cell Cultures (Wiltshire, U.K.) and stably transfected to overexpress MD2 as previously described.[32] Cells were cultured in DMEM supplemented with 10% heat-inactivated FBS and 0.1% blasticidin (10 µg at 37 °C in a 5% CO_2/air atmosphere).

Incubations. The cells were seeded in 12-well plates at 200000 cells/well to reach 90% confluence after 3 or 4 days. The cells were incubated in HEPES 0.1 M containing 1g/L of glucose with OCP1Cu (10 and 100 µM) and controls for 3 h (OCP1 10 and 100 µM, $CuSO_4$ 10 and 100 µM and bovine ZnCuSOD 100 U mL^{-1}). The supernatants were removed and cells were washed 2 times with PBS. Cells were then incubated with DMEM supplemented with 10% heat-inactivated FBS and 0.1% blasticidin and containing LPS (0.1 µg mL^{-1}) for 3h. Supernatants were collected and stored at 4 °C before enzyme-linked immunosorbent assay (ELISA) and lactate dehydrogenase (LDH) assays. The cells were washed with PBS and lysed in phosphate-buffered saline (PBS) containing a 1% Triton X-100 and protease inhibitors cocktail. They were harvested by scraping and stored at −20 °C before cytotoxicity, and protein quantification experiments.

Cytotoxicity. Cytotoxicity of the compounds was tested systematically for each experiment by following the release of the cytosolic lactate dehydrogenase (LDH) into the supernatant, indicating membrane damages, with a limit for non-cytotoxicity chosen at 10%. No cytotoxicity was observed in HT29-MD2 cells upon incubation, with or without LPS. The assay is based on the ability of LDH contained in cell lysates or supernatants to catalyze the reduction of pyruvate (0.6 mM) into lactate in the presence of NADH (0.18 mM), which is oxidized to form NAD+ in PBS. The level of LDH was proportional to amount of pyruvate consumed measured by monitoring the decrease in absorbance (340 nm) due to oxidation of NADH during 1 min. The percentage of LDH release in supernatants was calculated by dividing this LDH activity found in supernatant, by the sum of activity in supernatants and cell lysates.

Protein quantification. Protein concentrations were determined in cell lysates using BCA protein assay reagents and bovine serum albumin (BSA) as standard according to the manufacturer's instructions. Briefly, a disclosing solution (98% BCA, 2% $CuSO_4$) was added to the protein solution in 96-wells plate. After 30 min at 37°C, the absorbance was monitored at 560 nm in a SpectraMax M5e microplate reader from Molecular Devices. Absorbance was linked to protein mass thanks to a calibration curve with BSA.

IL8 quantification. Levels of IL8 produced by the cells were determined in cell supernatants using a commercially available ELISA kit according to the instructions of the manufacturer. The IL8 levels were normalized by the protein content determined in the corresponding cell lysates.

5. References

1 B. Bóka, A. Myari, I. Sóvágó and N. Hadjiliadis, *J. Inorg. Biochem.*, 2004, **98**, 113–122.

2 L. L. Costanzo, G. De Guidi, S. Giuffrida, E. Rizzarelli and G. Vecchio, *J. Inorg. Biochem.*, 1993, **50**, 273–281.

3 S. Kubota and J. T. Yang, *Proc. Natl. Acad. Sci.*, 1984, **81**, 3283–3286.

4 G. Csire, S. Timári, J. Asztalos, J. M. Király, M. Kiss and K. Várnagy, *J. Inorg. Biochem.*, 2017, **177**, 198–210.

5 A. Jancsó, Z. Paksi, N. Jakab, B. Gyurcsik, A. Rockenbauer and T. Gajda, *Dalton Trans.*, 2005, 3187.

6 D. Árus, A. Jancsó, D. Szunyogh, F. Matyuska, N. V. Nagy, E. Hoffmann, T. Körtvélyesi and T. Gajda, *J. Inorg. Biochem.*, 2012, **106**, 10–18.

7 S. Miriyala, I. Spasojevic, A. Tovmasyan, D. Salvemini, Z. Vujaskovic, D. St. Clair and I. Batinic-Haberle, *Biochim. Biophys. Acta BBA - Mol. Basis Dis.*, 2012, **1822**, 794–814.

8 M. F. J. M. Verhagen, E. T. M. Meussen and W. R. Hagen, *Biochim. Biophys. Acta BBA - Gen. Subj.*,

1995, **1244**, 99–103.
9 B. Bóka, A. Myari, I. Sóvágó and N. Hadjiliadis, *J. Inorg. Biochem.*, 2004, **98**, 113–122.
10 D. Sanna, C. Gábor Ágoston, I. Sóvágó and G. Micera, *Polyhedron*, 2001, **20**, 937–947.
11 C. Harford and B. Sarkar, *Acc. Chem. Res.*, 1997, **30**, 123–130.
12 K. P. Neupane, A. R. Aldous and J. A. Kritzer, *J. Inorg. Biochem.*, 2014, **139**, 65–76.
13 P. Gonzalez, K. Bossak, E. Stefaniak, C. Hureau, L. Raibaut, W. Bal and P. Faller, *Chem. – Eur. J.*, 2018, **24**, 8029–8041.
14 C. Hoffmann, D. Blechschmidt, R. Krüger, M. Karas and C. Griesinger, *J. Comb. Chem.*, 2002, **4**, 79–86.
15 M. Nitz, K. J. Franz, R. L. Maglathlin and B. Imperiali, *ChemBioChem*, 2003, **4**, 272–276.
16 C. Hoffmann, D. Blechschmidt, R. Krüger, M. Karas and C. Griesinger, *J. Comb. Chem.*, 2002, **4**, 79–86.
17 W. Liptay, *Z. Für Elektrochem. Berichte Bunsenges. Für Phys. Chem.*, 1962, **66**, 280–280.
18 H. Diebler, *Berichte Bunsenges. Für Phys. Chem.*, 1983, **87**, 1227–1227.
19 L. Zékány, I. Nagypál and G. Peintler, 1991.
20 A. Conte-Daban, V. Borghesani, S. Sayen, E. Guillon, Y. Journaux, G. Gontard, L. Lisnard and C. Hureau, *Anal. Chem.*, 2017, **89**, 2155–2162.
21 B. Alies, B. Badei, P. Faller and C. Hureau, *Chem. - Eur. J.*, 2012, **18**, 1161–1167.
22 M. Rance, *J. Magn. Reson. 1969*, 1987, **74**, 557–564.
23 J. Jeener, B. H. Meier, P. Bachmann and R. R. Ernst, *J. Chem. Phys.*, 1979, **71**, 4546–4553.
24 A. A. Bothner-By, R. L. Stephens, J. Lee, C. D. Warren and R. W. Jeanloz, *J. Am. Chem. Soc.*, 1984, **106**, 811–813.
25 T. L. Hwang and A. J. Shaka, *J. Magn. Reson. A*, 1995, **112**, 275–279.
26 G. Bodenhausen and D. J. Ruben, *Chem. Phys. Lett.*, 1980, **69**, 185–189.
27 R. E. Hurd and B. K. John, *J. Magn. Reson. 1969*, 1991, **91**, 648–653.
28 H. Kuthan, V. Ullrich and R. W. Estabrook, *Biochem. J.*, 1982, **203**, 551–558.
29 M. W. Sutherland and B. A. Learmonth, *Free Radic. Res.*, 1997, **27**, 283–289.
30 H. Y. V. Ching, I. Kenkel, N. Delsuc, E. Mathieu, I. Ivanović-Burmazović and C. Policar, *J. Inorg. Biochem.*, 2016, **160**, 172–179.
31 K. T. Kawagoe, J. A. Jankowski and R. Mark. Wightman, *Anal. Chem.*, 1991, **63**, 1589–1594.
32 E. Mathieu, A.-S. Bernard, N. Delsuc, E. Quévrain, G. Gazzah, B. Lai, F. Chain, P. Langella, M. Bachelet, J. Masliah, P. Seksik and C. Policar, *Inorg. Chem.*, 2017, **56**, 2545–2555.